Characterization and electronic structure calculations of the antiferromagnetic insulator Ca_3FeRhO_6

Volker Eyert and Udo Schwingenschlögl
TP II, Institut für Physik, Universität Augsburg, D-86135 Augsburg, Germany

Raymond Frésard, Antoine Maignan, Christine Martin, and Ninh Nguyen
Laboratoire CRISMAT, UMR CNRS-ENSICAEN(ISMRA) 6508, 6 Boulevard Maréchal Juin, 14050 Caen Cedex, France

Christian Hackenberger and Thilo Kopp
EP VI, Center for Electronic Correlations and Magnetism, Institut für Physik, Universität Augsburg, D-86135 Augsburg, Germany
(Received 4 October 2006; revised manuscript received 6 December 2006; published 6 March 2007)

We investigate the antiferromagnetic insulating nature of Ca_3FeRhO_6 both experimentally and theoretically. Susceptibility measurements reveal a Néel temperature of $T_N \simeq 20$ K and an effective magnetic moment of 5.3 μ_B/fu. Mössbauer spectroscopy strongly suggests that the Fe ions, located at trigonal prismatic sites, are in a 3+ high-spin state. Transport measurements display a simple Arrhenius law, with an activation energy of ~0.2 eV. The experimental results are interpreted with local spin-density approximation band-structure calculations, which confirm the Fe^{3+} state, the high-spin versus low-spin scenario, the antiferromagnetic ordering, and the value for the activation energy.

DOI: 10.1103/PhysRevB.75.115105 PACS number(s): 71.20.−b, 75.25.+z, 75.10.Pq, 75.50.Ee

I. INTRODUCTION

Interest in transition-metal oxides has never been restricted to the most spectacular phenomenon of the high-T_c superconductivity but also concerns, *inter alia*, metal-insulator transitions, colossal magnetoresistance, and magnetic and orbital orderings.[1] Among the numerous magnetic transitions that have been studied, most of them are associated with structural transitions.[2] In contrast, no anomalous temperature dependence of the structural parameters has been reported in the $m=0$ and $n=1$ members of the oxide family $A_{3n+3m}A'B_{3m+n}O_{9m+6n}$, which are currently attracting much attention.[3] These $A_3A'BO_6$ compounds crystallize in the K_4CdCl_6 structure, which consists of infinite chains along the c axis made of a 1:1 alternation of face-shared trigonal prisms $(A'O_6)_{TP}$ and octahedra $(BO_6)_{oct}$ (see, e.g., Refs. 4–7 for a detailed discussion of the crystal structure). According to their rhombohedral symmetry, the A cations separate the chains, the latter forming a hexagonal array. For such compounds, when the A' trigonal prism (TP) site is occupied by a magnetic cation, this provides interesting physical properties created by the coexistence of one-dimensionality character and geometrical frustration. This is illustrated by $Ca_3Co_2O_6$ for which the ordered antiferromagnetic state[4,5] below $T_N \sim 26$ K bears some similarity to the partially disordered antiferromagnetic (PDA) state, as originally proposed for ABX_3 geometrically frustrated one-dimensional (1D) compounds.[8] However, in marked contrast with the ABX_3 members, the intrachain coupling in $Ca_3Co_2O_6$ is ferromagnetic[4] and the magnetic-field-induced magnetization is very spectacular.[9–12] Indeed, as a function of the applied magnetic field, several magnetization jumps with a constant field spacing are observed. Besides, the saturation magnetization is larger than expected from the assumption of different spin states for Co^{3+} high spin (HS) and low spin (LS) at the trigonal prismatic and octahedral sites, respectively. Nonetheless, the ferromagnetic coupling along the chains is probably related to this "spin state ordering," the latter resulting from the different crystalline electrical fields in each Co^{3+} polyhedron. Such a coupling is likely to involve both LS Co^{3+} and O ions.[7,13,14] In that respect, the different magnetic behaviors of the two isostructural compounds Ca_3FeRhO_6 and Ca_3CoRhO_6 are worth mentioning.[15–22] In the latter, the ferromagnetic intrachain coupling is expected as Rh^{3+} is isoelectronic to Co^{3+} ($3d^6$), whereas the global magnetic behavior of Ca_3FeRhO_6 appears to be antiferromagnetic although Fe^{3+} (d^5) or Fe^{2+} (d^6) are both HS cations with large S values (5/2 or 2). Such different background states for the Ca_3MRhO_6 one–dimensional (1D) compounds (with M=Fe and M=Co) suggest subtle changes of the electronic structure.

In Ca_3FeRhO_6, contradicting results have been reported for the oxidation states of iron and rhodium cations, which add more complexity to the interpretation. In order to shed light on the magnetic and electronic behaviors of Ca_3FeRhO_6, we compare, in continuation of previous work,[23] results of band-structure calculations to the electrical and magnetic properties, together with Mössbauer spectroscopy measurements.

II. EXPERIMENTS

The polycrystalline sample of Ca_3FeRhO_6 was prepared by mixing the precursors CaO, Fe_2O_3, and Rh_2O_3 in the molar ratios of 3:0.5:0.5. The thoroughly mixed powder, pressed in bars ($\sim 2\times 2\times 10$ mm^3), was first heated at 900 °C for 24 h and then at 1250 °C for a 3×24 h period with intermediate x-ray controls. The crystallinity and purity of the obtained black and dense (>90%) product were checked by x-ray powder diffraction. The diffraction peaks have been indexed in the space group $R\bar{3}c$ with $a=9.1970(1)$ Å and c

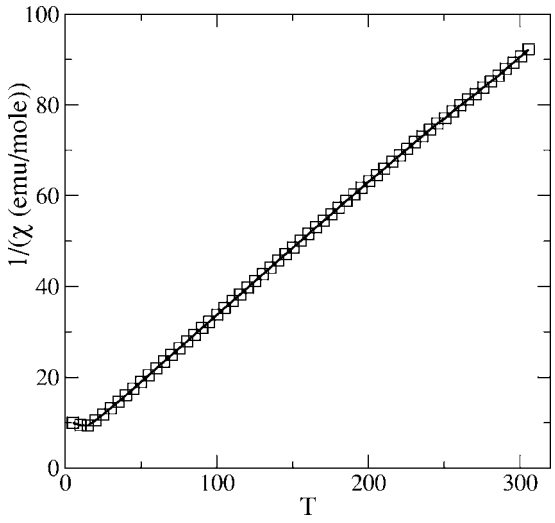

FIG. 1. Susceptibility of Ca_3FeRhO_6.

$=10.7888(1)$ Å in agreement with Refs. 15 and 16, allowing us to refine the 3:1:1 ratio for the cation Ca:Fe:Rh with an uncertainty of approximately 3% which is acceptable in all respects. Besides, small intensity peaks were also found, which could be attributed to $Ca_2Fe_2O_5$ (less than 1%). Magnetic measurements were performed with a superconducting quantum interference device magnetometer. Electrical resistivity was measured by the four-probe technique. The four electrical contacts were ultrasonically deposited on a bar. The measurements were made by using a physical properties measurement system (Quantum Design). Such resistivity measurements on dense ceramics yield good results as compared to those of crystals, as previously shown in the case of $Ca_3Co_2O_6$ polycrystalline and single crystals.[11,24] The ^{57}Fe powder Mössbauer resonance spectrum at room temperature was performed with a transmission geometry by the use of a constant acceleration spectrometer and a γ-ray source from ^{57}Co embedded in a rhodium matrix. The velocity scale was calibrated with an α-Fe foil at room temperature. The spectra were fitted with Lorentzian lines by the unpublished MOSFIT program. The isomer shift was referred to metallic α-Fe at 293 K.

III. RESULTS

A. Magnetism

When compared to the T-dependent reciprocal magnetic susceptibility curve $[\chi^{-1}(T)]$ of $Ca_3Co_2O_6$ as given in Ref. 25, the $\chi^{-1}(T)$ curve of Ca_3FeRhO_6 (Fig. 1) exhibits a much more linear behavior extending over a larger temperature range. This result reflects a lack of ferromagnetic interactions for the latter compound, as also attested by the different extrapolated temperatures for $\chi^{-1}(T=\theta_{CW})=0$, the Curie-Weiss temperature θ_{CW} values being -20 ± 1 and $+40\pm1$ K for Ca_3FeRhO_6 and $Ca_3Co_2O_6$, respectively. Furthermore, in $Ca_3Co_2O_6$ a χ^{-1} drop below $T_C\sim26$ K is observed, which indicates that a net ferrimagnetic state is reached: on each triangle made by three neighboring CoO_6 chains, two chains are antiferromagnetically coupled (zero net magnetic moment), whereas the third one exhibits a net ferromagnetic magnetization along the direction of the external applied magnetic field. In contrast, the $\chi^{-1}(T)$ curve of Ca_3FeRhO_6 exhibits a χ^{-1} increase below ~20 K indicative of a three-dimensional (3D) antiferromagnetic phase. Analysis of the slope along the linear region yields an effective paramagnetic moment $\mu_{eff}(\text{expt.})=(5.3\pm0.1)\mu_B/(\text{Fe+Rh})$. We will refer to this experimental value in Sec. III C.

TABLE I. Refined ^{57}Fe Mössbauer hyperfine parameters of Ca_3FeRhO_6 at room temperature including the linewidth Σ and %: relative intensity of the Mössbauer site.

IS (mm/s)	Σ (mm/s)	QS (mm/s)	%
0.45 (1)	0.28 (1)	1.20 (1)	96 (2)
0.73 (1)	0.36 (1)	1.49 (1)	4 (2)

The Mössbauer spectrum of this compound at room temperature consists of a paramagnetic doublet and is consistent with the measurements reported in Ref. 17. However, the best fit was obtained with two Mössbauer components, the hyperfine parameters of which are given in Table I. The observed isomer shift value ($IS=0.45\pm0.1$ mm/s) of the main component ($\%=96\pm2$) is typical of Fe^{3+} ions. Its high absolute quadrupole splitting value ($QS=1.20$ mm/s) shows that this site is not in the octahedral symmetry, and therefore the Fe ions are located in trigonal sites. For the minor Mössbauer component ($\%=4\pm2$), the IS value of 0.73 ± 0.1 mm/s rather corresponds to Fe^{2+} ions. Therefore, the vast majority of iron ions in Ca_3FeRhO_6 are in the trivalent state.

B. Transport

The second set of measurements concerns the expected localized nature of the electrical transport. Indeed, as shown in Table II, Ca_3FeRhO_6 appears far more insulating than the related Co compounds since, for instance, at 300 K, the resistivity ρ for Ca_3FeRhO_6 is 160 times larger than that of $Ca_3Co_2O_6$.[24] The T dependence of the resistivity confirms that Ca_3FeRhO_6 is insulating, as shown in Fig. 2. As T decreases, ρ increases very rapidly in Ca_3FeRhO_6, reaching the setup limit (corresponding to $\sim10^6$ Ω) at ~230 K. For the available temperature range, the linear $\ln\rho(T^{-1})$ curve shows that a simple Arrhenius law is followed from which an activation energy of 0.2 eV can be extracted. According to both, high ρ value and thermally activated behavior, it turns out that in Ca_3FeRhO_6 the charge carriers are localized. These large resistivity values cannot be explained by the presence of a secondary phase at the grain boundaries due to its small

TABLE II. Comparison of the resistivities at room temperature.

Compound	$Ca_3Co_2O_6$	Ca_3CoRhO_6	Ca_3FeRhO_6
ρ (300 K) (Ω cm)	50[a]	39[a]	8300

[a]Reference 24.

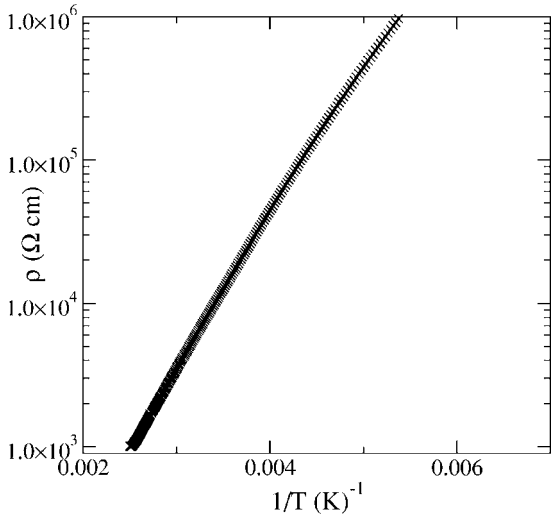

FIG. 2. Temperature dependence of the resistivity of Ca_3FeRhO_6, yielding an activation temperature $T_0=2200$ K.

amount, but is rather consistent with the antiferromagnetic intrachain coupling. These data for Ca_3FeRhO_6 confirm that despite the existing similarities to isostructural Ca_3CoRhO_6, i.e., the A'_{TP} and B_{oct} crystallographic sites are also occupied by trivalent cations with high spin ($S=5/2$ for Fe^{3+}) and low spin ($S=0$ for Rh^{3+}), respectively, the nature of the magnetic interactions differs strongly.

C. Band-structure calculations

For the local spin-density approximation (LSDA) band-structure calculations, we used the augmented spherical wave (ASW) method in its scalar-relativistic implementation.[26–28] In the ASW method, the wave function is expanded in atom-centered augmented spherical waves, which are Hankel functions and numerical solutions of Schrödinger's equation, respectively, outside and inside the so-called augmentation spheres. In order to optimize the basis set, additional augmented spherical waves were placed at carefully selected interstitial sites. The choice of these sites as well as the augmentation radii were automatically determined using the sphere-geometry optimization algorithm.[29] The Brillouin-zone integrations were performed using the linear tetrahedron method with up to 85 **k** points within the irreducible wedge. In contrast to our previous work,[23] we here use a new version of the ASW code, which takes the nonspherical contributions to the charge density inside the atomic spheres into account.[28]

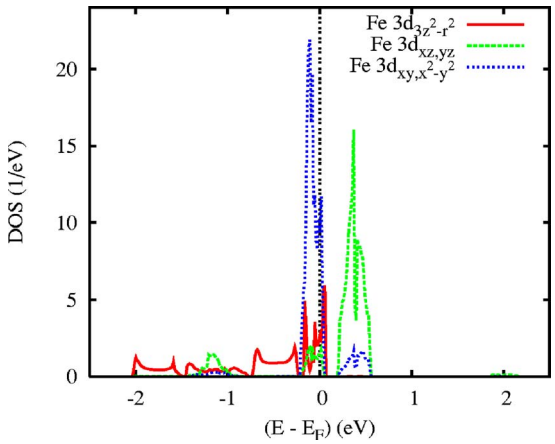

FIG. 4. (Color online) Partial Fe $3d$ DOS of spin degenerate Ca_3FeRhO_6.

All calculations are based on the powder data of Niitaka *et al.*[15] In a first step, we performed a set of calculations, where spin degeneracy was enforced. The resulting partial densities of states (DOSs) are shown in Fig. 3. While O $2p$ dominated bands are located in the interval from −6.8 to −2.4 eV, three groups of bands of mainly metal d character are found at higher energies. However, the strong d-p hybridization causes large p and d contributions, respectively, above and below −2 eV, reaching up to 50% especially for the Rh $4d$ states.

According to the partial Fe $3d$ densities of states shown in Fig. 4 the trigonal crystal field at the iron sites results in a splitting into nondegenerate $d_{3z^2-r^2}$ as well as doubly degenerate d_{xy,x^2-y^2} and $d_{xz,yz}$ states. The Rh $4d$ states as given in Fig. 5 experience a nearly perfect separation of the $4d$ states

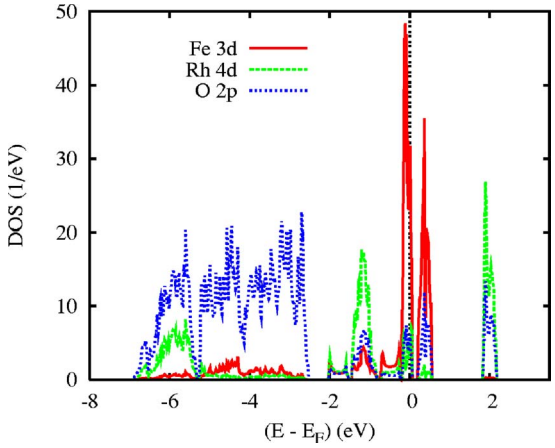

FIG. 3. (Color online) Partial densities of states (DOSs) of spin degenerate Ca_3FeRhO_6.

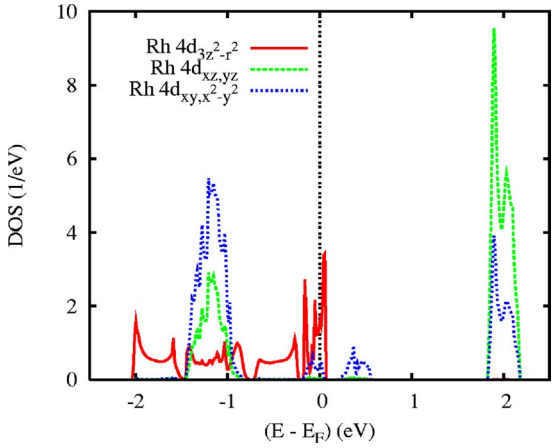

FIG. 5. (Color online) Partial Rh $4d$ DOS of spin degenerate Ca_3FeRhO_6.

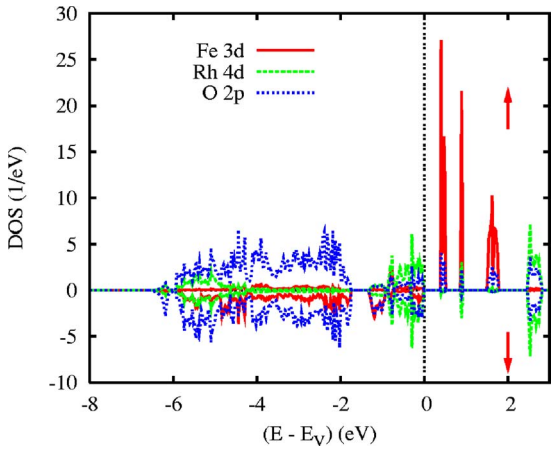

FIG. 6. (Color online) Partial DOS of antiferromagnetic Ca_3FeRhO_6.

into occupied t_{2g} and empty e_g states due to the octahedral crystal field at these sites. Whereas strong σ-type d-p bonding places the Rh $4d$ e_g states at 2.0 eV, the peak at about 0.4 eV traces back to Fe $4d_{xz,yz}$ states. For this reason, spin polarization of the latter bands is highly favorable, with the observed high-spin versus low-spin scenario.

In a second step, spin-polarized calculations were performed leading to the observed antiferromagnetic ordering, which is by 1 mRyd/Fe atom more stable than the ferromagnetic configuration. Well-localized magnetic moments of $0.00\mu_B$ (Rh), $3.77\mu_B$ (Fe), $0.13\mu_B$ (O), and $0.01\mu_B$ (Ca) are obtained in close agreement with those of previous calculations.[30] These values reflect the experimental result of low- and high-spin states at the octahedral and trigonal prismatic sites, respectively. The total moment per sublattice amounts to $\pm 4.58\mu_B$, which might be slightly altered by the inclusion of spin-orbit coupling, which is beyond the present work. The obtained total magnetic moment per sublattice, which corresponds to the saturation magnetization, is somewhat larger than that ($\approx 4.4\mu_B$, assuming a g factor of 2) calculated from the effective moment deduced from Fig. 1.

Worth mentioning are the rather high magnetic moments at the oxygen sites arising from the strong d-p hybridization, which sum up to about $0.8\mu_B$ per trigonal prism. Adding to the $3d$ moment, they lead to the formation of extended localized moments already observed in $Ca_3Co_2O_6$.[13] Our calculated $4.58\mu_B$ is, consequently, in favor of the Fe^{3+} $S=5/2$ configuration from which one expects a magnetic moment of $5\mu_B$ in the ordered magnetic state. The high-spin behavior at the iron sites is clearly observed in the partial DOS shown in Fig. 6, where the Fe $3d$ minority states display sharp peaks above E_F and the spin majority states are spread over a large energy interval as a result of the strong p-d hybridization.

The antiferromagnetic order growing out of the spin-polarized calculations goes along with the opening of an insulating gap of about 0.4 eV, as revealed by Fig. 6. This value corresponds to an activation energy of 0.2 eV, which is in remarkably good agreement with the experimental value deduced from Fig. 2.

IV. SUMMARY

In summary, we have performed susceptibility, Mössbauer spectroscopy, and transport measurements on the antiferromagnetic insulating compound Ca_3FeRhO_6. The experimental data have been compared with LSDA band-structure calculations, and the agreement is found to be very good. In particular, the calculations confirm several experimental key results as, e.g., the charge and spin states at the Fe and Rh sites including the characteristic high-spin versus low-spin scenario, the antiferromagnetic ordering, and the activation energy.

ACKNOWLEDGMENT

This work was supported by the Deutsche Forschungsgemeinschaft through SFB 484.

[1] S. Maekawa, T. Tohyama, S. E. Barnes, S. Ishihara, W. Koshibae, and G. Khaliullin, *Physics of Transition Metal Oxides* (Springer, Berlin, 2004).

[2] For a review, see *Colossal Magnetoresistance, Charge Ordering and Related Properties of Manganese Oxides*, edited by C. N. R. Rao and B. Raveau (World Scientific, Singapore, 1998); *Colossal Magnetoresistance Oxides*, edited by Y. Tokura (Gordon and Breach, London, 1999).

[3] K. E. Stitzer, J. Darriet, and H.-C. zur Loye, Curr. Opin. Solid State Mater. Sci. **5**, 535 (2001); V. Hardy, C. Martin, G. Martinet, and G. André, Phys. Rev. B **74**, 064413 (2006).

[4] H. Fjellvåg, E. Gulbrandsen, S. Aasland, A. Olsen, and B. Hauback, J. Solid State Chem. **124**, 190 (1996).

[5] S. Aasland, H. Fjellvåg, and B. Hauback, Solid State Commun. **101**, 187 (1997).

[6] U. Schwingenschlögl, Ph.D. thesis, Universität Augsburg, 2003; C. Hackenberger, Ph.D. thesis, Universität Augsburg, 2006.

[7] R. Frésard, C. Laschinger, T. Kopp, and V. Eyert, Phys. Rev. B **69**, 140405(R) (2004).

[8] M. Mekata, J. Phys. Soc. Jpn. **42**, 76 (1977); M. Mekata and K. Adachi, *ibid.* **44**, 806 (1978).

[9] H. Kageyama, K. Yoshimura, K. Kosuge, H. Mitamura, and T. Goto, J. Phys. Soc. Jpn. **66**, 1607 (1997).

[10] H. Kageyama, K. Yoshimura, K. Kosuge, M. Azuma, M. Takano, H. Mitamura, and T. Goto, J. Phys. Soc. Jpn. **66**, 3996 (1997).

[11] A. Maignan, C. Michel, A. C. Masset, C. Martin, and B. Raveau, Eur. Phys. J. B **15**, 657 (2000).

[12] A. Maignan, V. Hardy, S. Hébert, M. Drillon, M. R. Lees, O. Petrenko, D. McK. Paul, and D. I. Khomskii, J. Mater. Chem. **14**, 1231 (2004).

[13] V. Eyert, C. Laschinger, T. Kopp, and R. Frésard, Chem. Phys. Lett. **385**, 249 (2004).

[14] H. Wu, M. W. Haverkort, Z. Hu, D. I. Khomskii, and L. H. Tjeng, Phys. Rev. Lett. **95**, 186401 (2005).

[15] S. Niitaka, H. Kageyama, M. Kato, K. Yoshimura, and K. Kosuge, J. Solid State Chem. **146**, 137 (1999).

[16] M. J. Davis, M. D. Smith, and H. C. zur Loye, J. Solid State Chem. **173**, 122 (2003).

[17] S. Niitaka, K. Yoshimura, K. Kosuge, K. Mibu, H. Mitamura, T. Goto, J. Magn. Magn. Mater. **260**, 48 (2003).
[18] S. Niitaka, K. Yoshimura, K. Kosuge, M. Nishi, and K. Kakurai, Phys. Rev. Lett. **87**, 177202 (2001).
[19] S. Niitaka, K. Yoshimura, K. Kosuge, A. Mitsuda, H. Mitamura, and T. Goto, J. Phys. Chem. Solids **63**, 999 (2002).
[20] V. Hardy, M. R. Lees, A. Maignan, S. Hébert, D. Flahaut, and D. McK. Paul, J. Phys.: Condens. Matter **15**, 5737 (2003).
[21] S. Niitaka, H. Kageyama, K. Yoshimura, K. Kosuge, S. Kawano, N. Aso, A. Mitsuda, H. Mitamura, and T. Goto, J. Phys. Soc. Jpn. **70**, 1222 (2001).
[22] M. Loewenhaupt, W. Schäfer, A. Niazi, and E. V. Sampathkumaran, Europhys. Lett. **63**, 374 (2003).
[23] V. Eyert, U. Schwingenschlögl, C. Hackenberger, T. Kopp, R. Frésard, and U. Eckern, cond-mat/0509374, Prog. Solid State Chem. (to be published).
[24] A. Maignan, S. Hébert, C. Martin, and D. Flahaut, Mater. Sci. Eng., B **104**, 121 (2003).
[25] D. Flahaut, A. Maignan, S. Hébert, C. Martin, R. Retoux, and V. Hardy, Phys. Rev. B **70**, 094418 (2004); V. Hardy, D. Flahaut, R. Frésard, and A. Maignan, cond-mat/0701192, J. Phys.: Condens. Matter (to be published).
[26] A. R. Williams, J. Kübler, and C. D. Gelatt, Jr., Phys. Rev. B **19**, 6094 (1979).
[27] V. Eyert, Int. J. Quantum Chem. **77**, 1007 (2000).
[28] V. Eyert, *The Augmented Spherical Wave Method—A Comprehensive Treatment*, Lecture Notes in Physics (Springer, Heidelberg, 2007).
[29] V. Eyert and K.-H. Höck, Phys. Rev. B **57**, 12727 (1998).
[30] A. Villesuzanne and M.-H. Whangbo, Inorg. Chem. **44**, 6339 (2005).